Transfer-Learning-Assisted Multielement Calibration for Active Phased Antenna Arrays

Zhou, Zhao; Wei, Zhaohui; Ren, Jian; Yin, Yingzeng; Pedersen, Gert Frølund; Shen, Ming

Published in:
IEEE Transactions on Antennas and Propagation

DOI (link to publication from Publisher):
10.1109/TAP.2022.3216548

Publication date:
2023

Document Version
Accepted author manuscript, peer reviewed version

Communication

Transfer Learning assisted Multi-element Calibration for Active Phased Antenna Arrays

Zhao Zhou, Zhaohui Wei, Jian Ren, *Member, IEEE*, Yingzeng Yin, *Member, IEEE*, Gert Frølund Pedersen, *Senior Member, IEEE*, and Ming Shen, *Senior Member, IEEE*

***Abstract*—A transfer learning-based method for accelerating power-only calibration of phased array antennas by combining conventional array theory with deep learning is presented in this paper. Existing power-only calibration methods either require a significant number of measurement cycles or have restrictive phase shifter resolution requirements. The proposed array calibration method uses a surrogate model to calibrate all array elements in one pass without restricting phase resolution requirements. We developed a novel feature extraction scheme (FES) that picks out the most important power features resulting in reduced measurement cycles. The burden of data acquisition for model training is further reduced by relational knowledge transfer learning. The surrogate model acquires its general calibration capability from massive theoretical data, which is easily collected by the radiation multiplication theorem, and captures the detailed non-ideal response from a small number of simulations. The proposed methodology has been demonstrated and tested on several arrays for validation. The effectiveness and performance of the method have been verified, hence it can serve as a complementary tool to accelerate the calibration process of phased antenna arrays.**

***Index Terms*—calibration, feature extraction scheme, phased antenna array, transfer learning.**

I. Introduction

PHASED antenna arrays are becoming increasingly important and are widely used in wireless communication systems. They rely on precise control of array excitation. In practice, tolerances in component fabrication and aging effects can cause non-negligible distortions. The actual array excitation may deviate from the expected values and depreciate the performance. Therefore, regular calibration must be performed to maintain the performance.

The calibration methods can be divided into two groups: single-element and multi-element methods. The typical single-element methods calibrate only one element in one pass [1–7], and the extended multi-element methods calibrate multiple elements simultaneously during one calibration cycle [8–17]. Moreover, depending on the methodology, they can be further categorized as the mutual coupling-based method [1], the phase toggling method [2], [13], the rotating element electric field vector (REV) method [3–5], [14], [15], and the orthogonal code-based method, etc.

Since the typical single-element calibration methods [1–7] calibrate each element individually, an array antenna with N elements requires at least N calibration cycles. During each calibration cycle, a target element to be calibrated is activated and measured with different phase settings. Meanwhile, the remaining elements are isolated as they are turned off or terminated. Different calibration methods require measurement at different sets of phase settings.

The mutual coupling-based method [1] technically makes a phase adjustment during each measurement cycle. It measures the mutual coupling between the target and reference elements to determine the excitation error. The phase toggling method [2] switches the phase shifter from 0° to 180° and measures complex array signals to determine the error of each element. If the complex signals are not retrievable, the REV method is successful. The REV method [3–5] traverses all phase states of each element to determine the minimum and maximum power and the phase variation to determine the relative complex excitation field of the element. Typical REV methods require $2^m \times N$ measurement cycles to calibrate an N-element array with an m-bit phase shifter [4]. The phase resolution m must be at least 3 to achieve a clear sinusoidal representation.

The extended calibration methods [13–17] improve calibration efficiency by calibrating multiple elements simultaneously in each calibration cycle. Assuming M elements, a phased array antenna with N elements requires only $\lceil N/M \rceil$ measurement cycles. However, the number of elements in each calibration cycle is limited by the mathematical constraints and the number of bits of the phase shifter.

In [13], up to eight elements are calibrated simultaneously by applying a fast Fourier transform to sixteen measured signals, where the beamformer unit consists of sixteen phase states. The extended REV method [14], [15] successively shifts the phases of multiple elements with different phase intervals and measures the combined power change of the array. Then, the measured combined array power variation is converted into a form identical to the typical REV method using a Fourier transform.

While these extended methods improve the efficiency of calibration, still the improvement is limited due to the high mathematical computation requirements and phase resolution requirements. The number of elements calibrated simultaneously must be limited to ensure mathematical computation ability so that they provide independent contributions to the

Manuscript received XXX XX, XXXX; revised XXX XX, XXXX. This work was supported in part by the China Scholarship Council. Corresponding author: Ming Shen (mish@es.aau.dk) and Jian Ren (renjianroy@gmail.com).

Zhao Zhou, Zhaohui Wei, Gert Frølund Pedersen, and Ming Shen are with the Department of the Electronic Systems, Aalborg University, 9220 Aalborg, Denmark (e-mail: gfp@es.aau.dk; mish@es.aau.dk).

Jian Ren, and Ying Zeng Yin are with the National Key Laboratory of Antennas and Microwave Technology, Xidian University, Xi'an 710071, China.

Color versions of one or more of the figures in this communication are available online at https://ieeexplore.ieee.org.

Digital Object Identifier 00.0000/TAP.0000.0000000

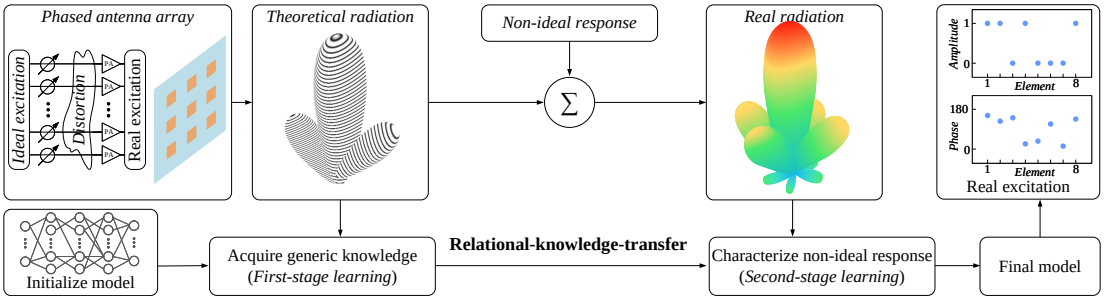

Fig. 1. The proposed calibration method based on the surrogate model.

composite array radiation and can be successfully decomposed. The bit-number of the phase shifter usually determines the ability to be independent. For this reason, the extended methods often have non-negotiable hardware requirements for the bit-number of the phase shifter. In the case of the classic extended REV method, only two elements can be calibrated simultaneously when using a 4-bit phase shifter.

In this communication, a surrogate model is proposed to calibrate all elements of a phased antenna array at once. It requires much fewer measurement cycles than the existing REVs. This powerful technique does not require phase resolution, phase tuning, on-off elements, and equation manipulation. The surrogate model feeds from a few power-only features measured under the default phase state and directly determines the complex excitation field. A feature extraction scheme (FES) was thoroughly investigated to filter out the most informative features while keeping number of features small. As a result, measurement cycles could be significantly reduced. Training of the surrogate model alleviates the tedious data acquisition that existing machine-learning approaches often suffer from [18–20]. Unlike [18–20], which output only amplitude or phase, our model determines both the excitation amplitudes as well as phases for calibration. As shown in Fig. 1, using relational-knowledge-transfer learning, we divide the model training into two stages. The first-stage learning acquires knowledge about the general calibration from the array superposition theorem. The second-stage learning focuses on unexpected concrete properties such as coupling effects and other non-analytical behavior. We have verified the effectiveness and efficiency of the proposed method on several arrays.

The remainder is organized as follows. Section II examines the FES for feature selection. Section III explains the development and optimization of the surrogate model. Validation of the proposed method is presented in Section IV while conclusion is drawn in Section V.

II. Feature Extraction Scheme

The input of the surrogate model is the features extracted by the feature extraction scheme (FES), while the output of the surrogate model is the complex excitation field. This section explains the FES to extract the fewest and most informative radiation features.

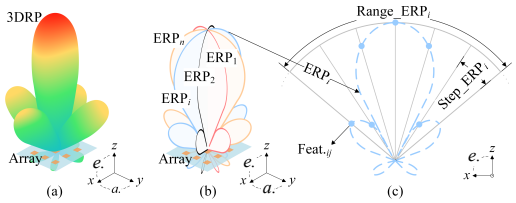

Fig. 2. (a) 3DRP; (b) ERPs; (c) Sampling the front region of an ERP.

A. Theoretical Basis

The phased antenna array regularly radiates according to two main rules: (a) the radiation intensity varies more dramatically with elevation (*e.*) angle θ than azimuth (*a.*) angle ϕ. Thus, the elevation radiation pattern (ERP) provides more informative features, and it is reasonable to represent radiation only by collecting multiple ERPs. And, (b) most of the energy is radiated forward, so the most important features of each ERP are mainly confined to the forward region.

B. Strategy of FES

The antenna array usually expresses its radiations in a three-dimensional far-field radiation pattern (3DRP) as shown in Fig. 2 (a). A small number of features result in a small number of measurement cycles and high calibration efficiency. The above analysis leads to a general strategy of the FES: capturing several ERPs and sampling the front range, as exhibited in Fig. 2 (b) and (c). We consider the radiation as a continuous function F versus the elevational angle θ and the azimuthal angle ϕ. Then each ERP can be expressed as $F_i(\theta, \phi_i)$. Each feature ($Feat_{ij}$) can be expressed as $F_{ij}(\theta_j, \phi_i)$, where θ_j is selected by both *Range_ERP* and *Step_ERP*. Here, *Num_ERPs* means the number of captured ERPs; *Range_ERP* defines the sampling range of each ERP; and *Step_ERP* decides the sampling intensity of each ERP. They customize the FES and decide the number of features (*Num_Feats*).

C. The Optimal FES

FES can be parameterized by three coefficients, i.e., *Range_ERP*, *Step_ERP*, and *Num_Feats*. Variation in these coefficients results in different FESs. There are two indicators to assess an FES, one is *Num_Feats* and the other is the consequent surrogate model's loss represented as L. Roughly, fewer features lead to worse performance. To quantify the

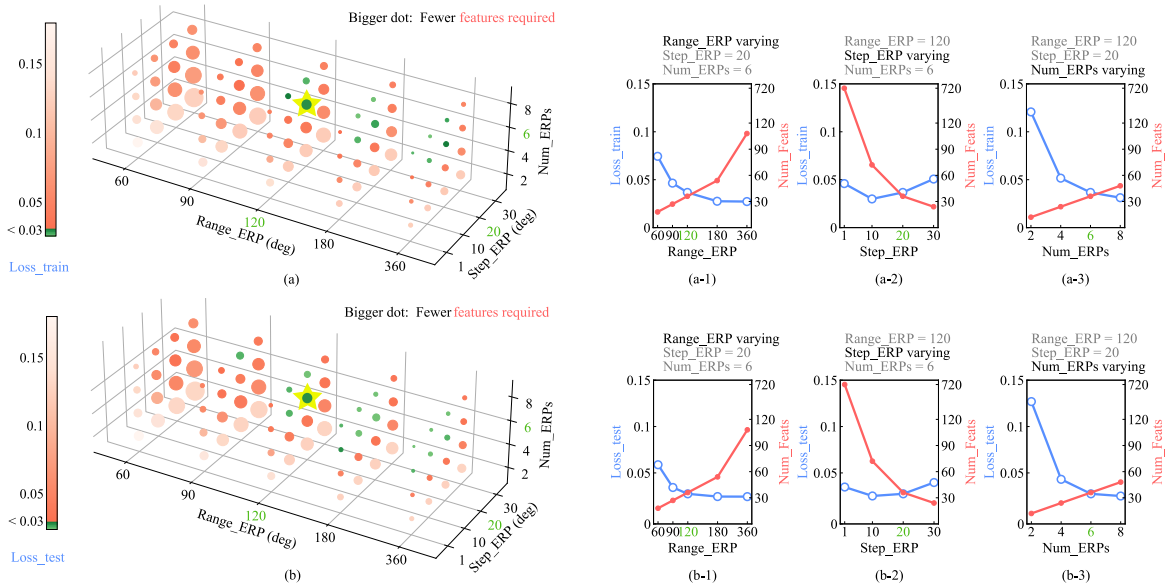

Fig. 3. *Loss_train* with (a) *Num_ERPs*, *Range_ERP*, and *Step_ERP* varying, (a-1) *Range_ERP* varying, (a-2) *Step_ERP* varying, (a-3) *Num_ERPs* varying; *Loss_test* with (b) *Num_ERPs*, *Range_ERP*, and *Step_ERP* varying, (b-1) *Range_ERP* varying, (b-2) *Step_ERP* varying, (b-3) *Num_ERPs* varying.

trade-off between the two indicators, we evaluated 80 different FESs.

For simplicity and fairness, the fifty thousand samples are used by 80 different FESs to generate 80 corresponding training data sets. A deep neural network is trained separately with the 80 data sets. During training, the mean squared error between the prediction and label of the complex excitation field was set as the loss function. The final loss represents L.

The colored dots of different sizes represents the 80 FESs in Fig. 3 (a) and (b). Here, the size indicates the number of features (*Num_Feats*) required as the bigger dot corresponds to the small number of required features. Whereas, the color represents the loss value as green means the loss value meets certain criteria (less than 0.03). The green color transforms to orange and gradually lighter orange as the loss value increases. Note that the threshold value for testing exceeds for training because models often behave slightly inferior during testing. It can be observed that the biggest green dots in Fig. 3 (a) and (b) represent the optimal FES (*Num_ERPs* $= 6$, *Range_ERP* $= 120$, *Step_ERP* $= 20$).

The $2D$ plots on the right of Fig. 3, shows the trade-off when two of the coefficients are fixed at their optimal values. Fig. 3 (a-1), (a-2), and (a-3) represents trade-off for training while Fig. 3 (b-1), (b-2), and (b-3) shows trade-off for testing. According to the optimal FES, six ERPs and six far-field radiation values on each ERP are selected as the input parameters for the surrogate model.

For larger uniform planar arrays, the number of ERPs and the fineness of the FES proportionally rise to deliver the radiation of higher resolution. For non-uniform arrays with special arrangements, there is the need to adjust the ERPs distribution accordingly to fit the radiation distribution. The number of candidate FESs depends on the sweep ranges of *Num_ERPs*, *Range_ERP*, and *Step_ERP*.

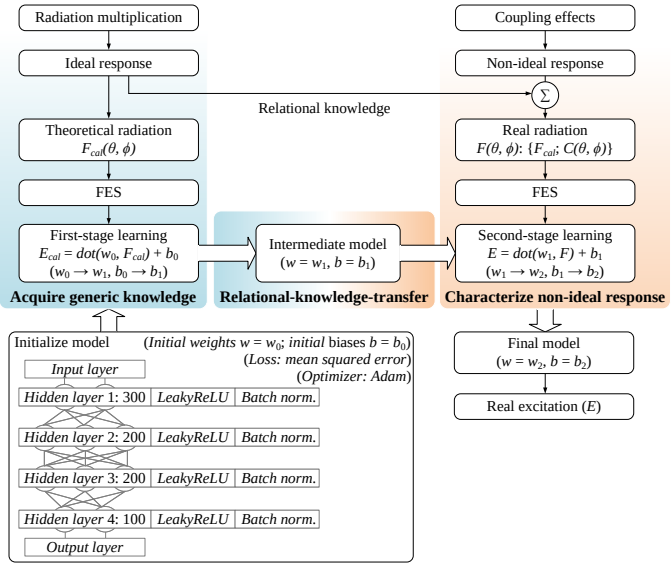

Fig. 4. The workflow to develop the surrogate model.

III. The Surrogate Model

A. Workflow

The evolution of the surrogate model, as illustrated in Fig. 4, arises from combining the conventional array theory and deep learning. The purpose of the surrogate model is to imitate the mapping from the power-only far-field radiation values to the excitation field. The mapping has its general relationship decided by the radiation multiplication theorem, and the coupling effects mainly generate undesirable variations.

The model can learn the generic knowledge of the radiation multiplication from theoretical calculation results; however, the non-ideal response originated from the coupling effects only exposes itself in simulation or measurement results. Thus, the relational-knowledge-transfer approach is used to

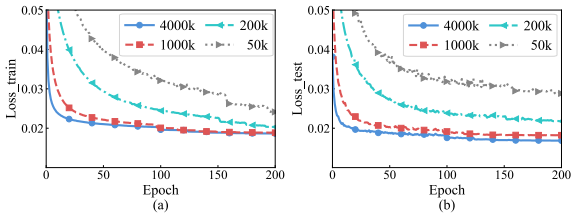

Fig. 5. Loss versus epochs during the first stage using different amounts of calculation datasets. (a) Loss_train. (b) Loss_test.

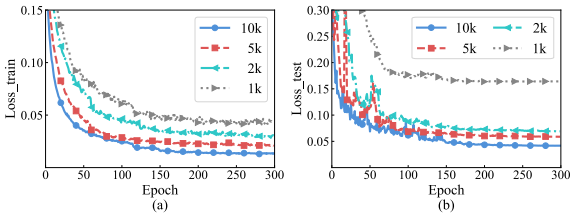

Fig. 6. Loss versus epochs during the second stage using different amounts of simulation datasets. (a) Loss_train. (b) Loss_test.

decompose the learning process into two stages. The first-stage learning grasps the generic knowledge from theoretical calculation results. The second-stage learning further characterizes the detailed non-ideal variations from a few simulation results.

This two-stage learning mode renders the model having generalizability, robustness, and interpretability. Also, our approach improves efficiency by significantly alleviating the need for stimulation by transferring knowledge from the calculation. The following section introduces the first/second-stage learning.

B. Acquire Generic Knowledge

After fine tuning and optimization, a fully-connected neural network is initialized, as shown in Fig. 4, which consists of an input layer, an output layer, and four hidden layers of 300, 200, 200, and 100 neurons. Each hidden layer is attached with the leaky rectified linear unit (LeakyReLU) [21] as the activation function and a batch normalization layer. The Adam [22] is employed as the optimizer to upgrade the weights and biases of the neurons. The mean squared error between the predicted complex excitation field and its theoretical label is used as the loss function to evaluate the model during training.

In the first stage, the model is trained with theoretical data to grasp the generic knowledge where the deviations were excluded. The theoretical data were obtained via the formula established in [23]:

$$F_{cal}(\theta,\phi)=\sum_{m=0}^{M-1}\sum_{n=0}^{N-1}F_{e,mn}(\theta,\phi)e^{-j\pi\sin\theta(m\cos\phi+n\sin\phi)}. \quad (1)$$

Here, $F_{e,mn}(\theta,\phi)$ represents the independent radiation pattern of the antenna element; *m* and *n* point at the index of the antenna element in two orthogonal directions while *M* and *N* are the numbers of the elements along with these two directions. The unbalanced magnitudes and phases for all the elements were initialized to generate the first-stage training data and then fed into the Eq. 1 to calculate the theoretical array of radiation. The amplitude can be deviated by $\pm 3\,\mathrm{dB}$, and the phase varies from $-40\,^\circ$ to $40\,^\circ$. The theoretical array radiation was the input, and the initialized magnitudes and phases were its output label.

The training and testing loss convergence curves versus the learning epoch are exhibited in Fig. 5. Here, the loss indicates the mean squared error between the first-stage model estimation and the theoretical label of the complex excitation field. Generally, more data results in minor loss, consequently better performance. Nevertheless, this improvement is saturated when the data size reaches four million, as in Fig. 5, and the curves indicate that four million could ensure good performance. Hence, four million calculation results are used for the first-stage training. After the first-stage learning, the initial model is referred as the intermediate model which has learned the generic knowledge of radiation multiplication.

C. Characterize Non-ideal Response

The second-stage learning focuses on characterizing the detailed non-ideal response, including the coupling effects and other non-analytical behavior. This stage relies on the learning by the intermediate model as it holds the generic calibration knowledge. Therefore, in the second stage, the aim is to capture the non-ideal characteristics due to mutual coupling and other non-analytical behavior. Similarly, the mean square error between the second-stage prediction and the simulation of the complex excitation field is set as the loss function for evaluating the second-stage model.

Alike the first stage, then unbalanced magnitudes and phases for all elements were initialized and randomly chosen for the second-stage data collection. They are fed into the simulation setup supported by Computer Simulation Technology®(CST) to yield the non-ideal array radiation. A few arbitrary elements had the amplitudes deviated by $\pm 3\,\mathrm{dB}$, and the phases varied from $-40\,^\circ$ to $40\,^\circ$. The simulated array radiation was the input, and the initialized magnitudes and phases were its output.

Following this scheme, the model was trained with different numbers of simulation results as shown in Fig. 6. Here, the loss represented the mean squared error between the simulated magnitudes and phases and the output during the second-stage iterations. As indicated by the curves, ten thousand simulation data are sufficient for the second-stage learning.

IV. Validation and Discussion

A. Virtual Validation

The proposed method is applied on a three-by-three planar phased patch antenna array to verify its effectiveness and performance. At first, arbitrary excitation distortions were pre-imposed on the array as amplitudes were deviated by $\pm 3\,\mathrm{dB}$, and phases deviated from $-40\,^\circ$ to 40°.

The optimal FES consisted of six ERPs. For each ERP, six power radiation points within the front region were collected. The collected features were fed into the well-established surrogate model to determine the actual excitation. Fig. 7 exhibits

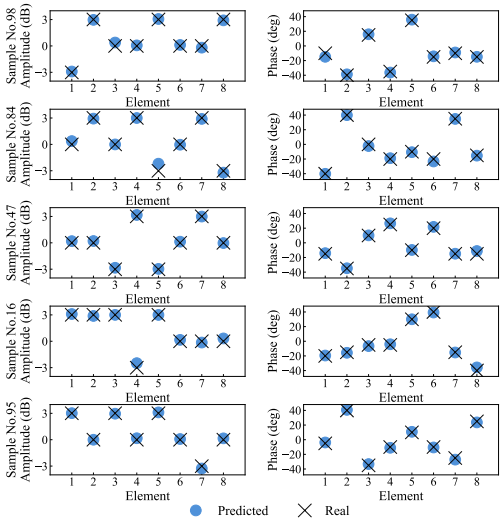

Fig. 7. Implementation A: 5 samples randomly chosen from 100 cases.

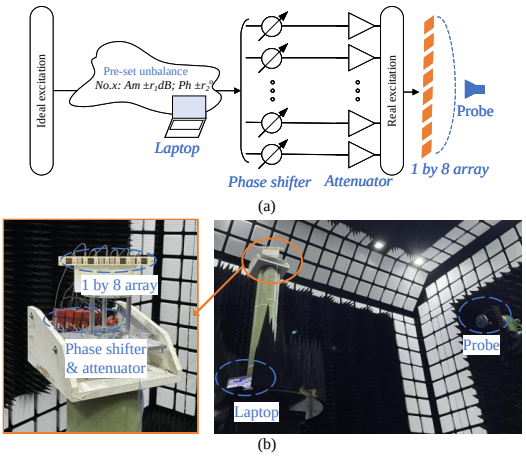

Fig. 8. (a) Schematic diagram of the measurement setup. (b) Photograph of the measurement setup in an anechoic chamber.

5 validation samples randomly chosen from 100 validation cases. The well-trained model is validated with 100 different unbalanced samples. The root mean square errors (RMSEs) of amplitude and phase of the 100 validation cases are $0.36\,\mathrm{dB}$ and $4.51\,^\circ$. As observed, the proposed surrogate model can precisely determine the unbalanced variations in amplitude and phase.

The method is firstly verified using a virtual scenario in a similar manner to other existing machine learning-based works [19], [20]. The measurement results agree with the simulation via CST as long as the setup is accurate. It is worth mentioning that a three-by-three phased antenna array was chosen to balance the time and computing recourse needed for validation and the complexity level of the array.

B. Experimental Validation

The robustness of the proposed method is validated by implementing it on a one-by-eight linear patch array at 3.5 GHz in an experimental scenario. The experimental setup is shown in Fig. 8, with a one-by-eight linear patch array, 8 $Vaunix\ LPS{-}402$ phase shifters, a $Vaunix\ LDA{-}906V{-}8$ 8-channel attenuator, an 8-channel power divider, and a laptop to adjust the phase shifters and attenuator all placed in an anechoic chamber of $14\,\mathrm{m}\times9.9\,\mathrm{m}\times11.05\,\mathrm{m}$. The elements are aligned in $\phi = 0^\circ$ direction. Therefore, only took one ERP $\phi = 0^\circ$ was taken and had 32 features within this ERP because the radiation variation focused in the ERP of $\phi = 0^\circ$.

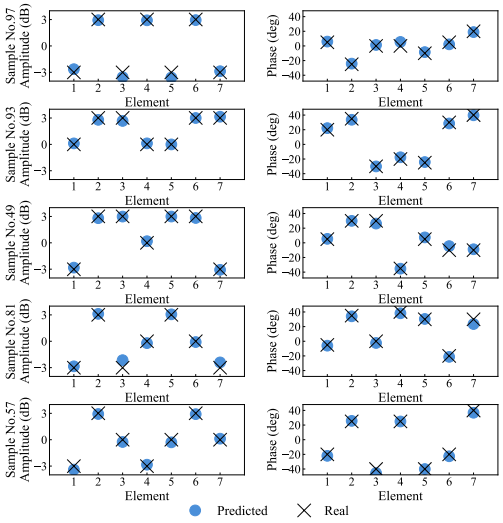

Fig. 9. Implementation B: 5 samples randomly chosen from 100 cases.

We measured 100 unbalanced far-field array radiations in the chamber. The RMSE of 100 calibration results in the linear array case is $0.47\,\mathrm{dB}/5.37\,^\circ$ in terms of amplitude/phase. Fig. 9 exhibits 5 random cases. The increment of error depends on the accuracy of measurement.

C. Large Array Validation

The proposed method has the potential to calibrate any large arrays with sufficient training samples available. The main challenge is that, as the array size increases, the number of required training samples and the training time arise significantly because the number of possible array excitation combinations arises exponentially. In these validations, amplitudes were deviated by $\pm3\,\mathrm{dB}$, and phases from $-30\,^\circ$ to $30\,^\circ$.

It was applied on a four-by-four planar array, with the FES of *Range_ERP*=180°, *Step_ERP*=22.5°, and *Num_ERPs*=8. 4×10^7 samples were used for training, and the RMSE was $0.57\,\mathrm{dB}/6.14\,^\circ$ in terms of amplitude/phase.

For a linear array of 32 elements, the FES was set as *Range_ERP*=120°, *Step_ERP*=1°, and *Num_ERPs*=1. After being trained using 4×10^8 samples, the RMSE for 10 thousand test samples is $0.62\,\mathrm{dB}/6.65\,^\circ$ in terms of amplitude/phase.

For a four-by-eight planar array, the FES was fixed at *Range_ERP*=180°, *Step_ERP*=15°, and *Num_ERPs*=10. It took 8×10^8 samples for training to arrive at the RMSE of $0.67\,\mathrm{dB}/6.84\,^\circ$ for 10 thousand test samples. Planar arrays require more training samples than linear arrays of the same amount of elements, because planar arrays have to consider more complex $3D$ radiation variations than linear ones.

The propoosed method has the potential to calibrate larger arrays and the calibration loss can be further reduced if more

TABLE I
THE COMPARISON BETWEEN THE PROPOSED METHOD AND THE EXISTING POWER-ONLY METHODS

	Measurement times	Root mean square error (Amplitude/Phase)	phase shifter
[4]	$2^m \times N$	– / –	m-bit
[5]	$4.5N + 1$	0.1087 / 4.754°	4-bit
[15]	$11.2N$	$0.37\,\mathrm{dB}$ / 3.06°	5-bit
This work	**4*N***	**0.07 (0.36 dB) / 4.51°**	**No requirement**
	4*N*	**0.10 (0.47 dB) / 5.37°**	**No requirement**

data and more powerful computing resources are provided. However, powerful computing resources are not commonly available. In future work, we will focus on reduction of required training samples and the need for computing resources to facilitate large array calibration.

D. Comparison and Discussion

The proposed method is compared with existing ones in Table I. As authors in [4] claimed, a normal REV requires 2^m measurement times to calibrate each element using an m-bit phase shifter. Works in [5] and [15] reduced the average measurement cycles to around 4.5 and 11.2 by handling multiple elements simultaneously using 4 or 5-bit number phase shifters. Our method achieved comparable calibration accuracy with only 4 measurement cycles. Furthermore, it does not require phase shift resolution, repetitive phase shifting, or equation manipulation.

Theoretically, the proposed method can calibrate larger arrays by proportionally refining the FES. Consequently, the measurement cycles arise proportionally. The number of required training samples increases exponentially to provide sufficient informativeness and can exceeds the available computing memory as the array size grows. In future work, we will focus on further reduction of measurement cycles and data requirements to facilitate calibration of larger-scaled arrays in $5G/6G$ scenarios.

V. CONCLUSION

In this communication, a calibration technique is presented using the surrogate model that can calibrate all the elements of phased antenna arrays at once. The surrogate model gets insights from the combination of conventional array theory and deep learning and gains its calibration ability through relational-knowledge-transfer learning. The proposed method requires a smaller number of measurement cycles than the existing REVs and avoids repetitive phase shifting or equation manipulation. The experimental results show that the approximation of the measurement times is $4N$. The optimal FES distinguishes the fewest points that deliver the most informative power-only features. Fed by these features, the surrogate model can directly determine amplitudes and phases for all the elements. It also breaks through the limitation that the conventional extended methods suffer from the bit-number of the phase shifter or the mathematical computability. Once trained, the surrogate model can serve convenient and efficient periodical calibration for phased antenna arrays in $5G/6G$ scenarios.

VI. ACKNOWLEDGMENT

The authors would like to thank Kim Olesen for his experiment support.

REFERENCES

[1] H. Pawlak and A. F. Jacob, "An external calibration scheme for dbf antenna arrays," *IEEE Trans. Antennas Propag.*, vol. 58, no. 1, pp. 59–67, 2009.
[2] K.-M. Lee, R.-S. Chu, and S.-C. Liu, "A built-in performance-monitoring/fault isolation and correction (pm/fic) system for active phased-array antennas," *IEEE Trans. Antennas Propag.*, vol. 41, no. 11, pp. 1530–1540, 1993.
[3] M. Tanaka, "On-orbit measurement of phased arrays in satellites by rotating element electric field vector method," *Electron. Commun. Jpn.*, vol. 81, no. 1, pp. 1–13, 1998.
[4] T. Takahashi, H. Miyashita, Y. Konishi, and S. Makino, "Theoretical study on measurement accuracy of rotating element electric field vector (rev) method," *Electron. Commun. Jpn.*, vol. 89, no. 1, pp. 22–33, 2006.
[5] H.-J. Yoon and B.-W. Min, "Improved rotating-element electric-field vector method for fast far-field phased array calibration," *IEEE Trans. Antennas Propag.*, vol. 69, no. 11, pp. 8021–8026, 2021.
[6] G. He, X. Gao, and H. Zhou, "Fast phased array calibration by power-only measurements twice for each antenna element," *Int. J. Antennas Propag.*, vol. 2019, 2019.
[7] C.-N. Hu, "A novel method for calibrating deployed active antenna arrays," *IEEE Trans. Antennas Propag.*, vol. 63, no. 4, pp. 1650–1657, 2015.
[8] B. C. Ng and C. M. S. See, "Sensor-array calibration using a maximum-likelihood approach," *IEEE Trans. Antennas Propag.*, vol. 44, no. 6, pp. 827–835, 1996.
[9] W. T. Patton and L. H. Yorinks, "Near-field alignment of phased-array antennas," *IEEE Trans. Antennas Propag.*, vol. 47, no. 3, pp. 584–591, 1999.
[10] S. H. Son, S. Y. Eom, S. I. Jeon, and W. Hwang, "Automatic phase correction of phased array antennas by a genetic algorithm," *IEEE Trans. Antennas Propag.*, vol. 56, no. 8, pp. 2751–2754, 2008.
[11] M. D. Migliore, "A compressed sensing approach for array diagnosis from a small set of near-field measurements," *IEEE Trans. Antennas Propag.*, vol. 59, no. 6, pp. 2127–2133, 2011.
[12] C. He, X. Liang, J. Geng, and R. Jin, "Parallel calibration method for phased array with harmonic characteristic analysis," *IEEE Trans. Antennas Propag.*, vol. 62, no. 10, pp. 5029–5036, 2014.
[13] G. A. Hampson and A. B. Smolders, "A fast and accurate scheme for calibration of active phased-array antennas," in *IEEE Antennas Propag. Society Int. Symp. Dig.*, vol. 2. IEEE, 1999, pp. 1040–1043.
[14] M. Liu and Z. Feng, "Combined rotating-element electric-field vector (crev) method for nearfield calibration of phased array antenna," in *Int. Conf. Microw. Milli. Technol.* IEEE, 2007, pp. 1–4.
[15] T. Takahashi, Y. Konishi, S. Makino, H. Ohmine, and H. Nakaguro, "Fast measurement technique for phased array calibration," *IEEE Trans. Antennas Propag.*, vol. 56, no. 7, pp. 1888–1899, 2008.
[16] W. P. Keizer, "Fast and accurate array calibration using a synthetic array approach," *IEEE Trans. Antennas Propag.*, vol. 59, no. 11, pp. 4115–4122, 2011.
[17] Z. Wang, F. Zhang, H. Gao, O. Franek, G. F. Pedersen, and W. Fan, "Over-the-air array calibration of mmwave phased array in beam-steering mode based on measured complex signals," *IEEE Trans. Antennas Propag.*, 2021.
[18] R. G. Ayestaran, F. Las-Heras, and L. F. Herran, "High-accuracy neural-network-based array synthesis including element coupling," *IEEE Antennas Wireless Propag. Lett.*, vol. 5, pp. 45–48, 2006.
[19] R. Lovato and X. Gong, "Phased antenna array beamforming using convolutional neural networks," in *IEEE Int. Symp. Antennas Propag. USNC-URSI Radio Sci. Meet.* IEEE, 2019, pp. 1247–1248.
[20] J. H. Kim and S. W. Choi, "A deep learning-based approach for radiation pattern synthesis of an array antenna," *IEEE Access*, vol. 8, pp. 226 059–226 063, 2020.
[21] A. L. Maas, A. Y. Hannun, A. Y. Ng *et al.*, "Rectifier nonlinearities improve neural network acoustic models," in *Proc. Int. Conf. Mach. Learn.*, vol. 30, no. 1, 2013.
[22] D. P. Kingma and J. Ba, "Adam: A method for stochastic optimization," in *Int. Conf. Learn. Repr., ICLR, San Diego, CA, USA*, Y. Bengio and Y. LeCun, Eds., 2015.
[23] R. E. Collin, *Antenna theory*. McGraw-Hill, 1969, no. 1.